

Response of atmospheric pCO₂ to a strong AMOC weakening under climate change

A. A. Boot¹, A. S. von der Heydt^{1,2}, and H. A. Dijkstra^{1,2}

¹Institute for Marine and Atmospheric research Utrecht, Department of Physics, Utrecht University,

Utrecht, the Netherlands

²Center for Complex Systems Studies, Utrecht University, Utrecht, the Netherlands

Key Points:

- First results on the carbon cycle response to AMOC weakening in a CMIP6 Earth System Model are presented.
- Strong weakening of the AMOC does not result in a large response of atmospheric pCO₂ under climate change.
- The spatial patterns of the carbon cycle response to an AMOC weakening are not dependent on cumulative CO₂ emissions.

14 **Abstract**

15 The Earth System is warming due to anthropogenic greenhouse gas emissions which in-
 16 creases the risk of passing a tipping point in the Earth System, such as a collapse of the
 17 Atlantic Meridional Overturning Circulation (AMOC). An AMOC weakening can have
 18 large climate impacts which influences the marine and terrestrial carbon cycle and hence
 19 atmospheric pCO₂. However, the sign and mechanism of this response are subject to un-
 20 certainty. Here, we use a state-of-the-art Earth System Model, the Community Earth
 21 System Model v2 (CESM2), to study the atmospheric pCO₂ response to an AMOC weak-
 22 ening under low (SSP1-2.6) and high (SSP5-8.5) emission scenarios. A freshwater flux
 23 anomaly in the North Atlantic strongly weakens the AMOC, and we simulate a weak pos-
 24 itive pCO₂ response of 0.45 and 1.3 ppm increase per AMOC decrease in Sv for SSP1-
 25 2.6 and SSP5-8.5, respectively. For SSP1-2.6 this response is driven by both the oceanic
 26 and terrestrial carbon cycles, whereas in SSP5-8.5 it is solely the ocean that drives the
 27 response. However, the spatial patterns of both the climate and carbon cycle response
 28 are similar in both emission scenarios over the course of the simulation period (2015-2100),
 29 showing that the response pattern is not dependent on cumulative CO₂ emissions up to
 30 2100. Though the global atmospheric pCO₂ response might be small, locally large changes
 31 in both the carbon cycle and the climate system occur due to the AMOC weakening, which
 32 can have large detrimental effects on ecosystems and society.

33 **Plain Language Summary**

34 The Atlantic Meridional Overturning Circulation (AMOC) modulates global cli-
 35 mate by transporting heat from the Southern to the Northern Hemisphere. The AMOC
 36 is considered to be a tipping element with a possible future collapse under climate change.
 37 An AMOC weakening can have large climate impacts which influences the marine and
 38 terrestrial carbon cycle and hence the atmospheric pCO₂. Here, we use a state-of-the-
 39 art Earth System Model to study the atmospheric pCO₂ response to an AMOC weak-
 40 ening under low and high emission scenarios. We use simulations where we artificially
 41 weaken the AMOC, which results in a weak positive response of 0.45 and 1.3 ppm pCO₂
 42 increase per decrease in Sv for low and high emissions, respectively. For low emissions
 43 this response is driven by both the oceanic and terrestrial carbon cycle processes, whereas
 44 in the high emission scenario it is solely the ocean that drives the response. Spatial pat-
 45 terns, both the climate and carbon cycle response, are similar in both emission scenar-
 46 ios over the course of the simulation period (2015-2100). The global atmospheric pCO₂
 47 response is small, but locally large changes in both the carbon cycle and the climate sys-
 48 tem can occur due to the AMOC weakening.

49 **1 Introduction**

50 Anthropogenic emissions of greenhouse gases cause the Earth System to change and
 51 warm up. As temperatures increase, we are at risk of crossing tipping points with pos-
 52 sibly large detrimental effects on our climate, biodiversity and human communities (Lenton
 53 et al., 2008; McKay et al., 2022). One of these tipping points can occur in the Atlantic
 54 Meridional Overturning Circulation (AMOC) (Lenton et al., 2008). Currently, the AMOC
 55 is in a so-called on-state where it transports heat from the Southern Hemisphere to the
 56 Northern Hemisphere and thereby modulates global and especially European climate (Buckley
 57 & Marshall, 2016). In models, the AMOC can be strongly weakened and in this so-called
 58 collapsed state (or off-state), the northward heat transport is disrupted with large global
 59 climatic effects (Orihuela-Pinto et al., 2022).

60 Proxy-based evidence suggest that AMOC collapses have occurred frequently dur-
 61 ing the Pleistocene where they are a main source of millennial variability (e.g. the Dansgaard-
 62 Oeschger cycles; Rahmstorf, 2002; Lynch-Stieglitz, 2017). The disrupted heat transport
 63 causes warming of surface air temperature (SAT) and sea surface temperature (SST) in

the Southern Hemisphere, while the Northern Hemisphere cools (also called the ‘bipolar seesaw’; Vellinga & Wood, 2002; Caesar et al., 2018), with local SAT changes up to 10°C (Cuffey & Clow, 1997; Rahmstorf, 2002). In models, the bipolar seesaw results in an increased northern hemispheric sea-ice extent and changes in atmospheric dynamics (Vellinga & Wood, 2002; Orihuela-Pinto et al., 2022). The changes in atmospheric dynamics are, for example, seen in wind fields with strengthened trade winds and strengthened Pacific Walker Circulation (Orihuela-Pinto et al., 2022), and a southward shift of the Intertropical Convergence Zone (ITCZ) (Zhang & Delworth, 2005; Jackson et al., 2015). The tipping threshold for the AMOC is estimated to be around 4 °C of warming relative to pre-industrial climate (McKay et al., 2022).

In addition to the climate system, also the carbon cycle is affected by an AMOC collapse. In the ocean, the change in ocean circulation affects the advection of important tracers such as Dissolved Inorganic Carbon (DIC) and nutrients (Zickfeld et al., 2008). An AMOC collapse can also change upwelling rates and surface stratification, processes that are important for driving Net Primary Production (NPP) and carbon sequestration in the deep ocean. Terrestrial primary productivity is affected by the changing temperature and precipitation patterns. Locally, this can lead to both a reduction or an increased uptake of CO₂ (e.g. Köhler et al., 2005). Several studies have looked into a potential feedback between AMOC dynamics and atmospheric pCO₂, which is controlled by the exchange of the atmosphere with the ocean and land carbon stocks. These studies (e.g. Marchal et al., 1998; Köhler et al., 2005; Schmittner & Galbraith, 2008), mostly focused on Pleistocene and pre-industrial conditions, show a wide range of possible responses. There is no clear consensus on the responses of the terrestrial and ocean carbon stock to an AMOC weakening, or to the net effect on atmospheric pCO₂, which can be attributed to different climatic boundary conditions, timescales assessed, and model detail used (Gottschalk et al., 2019). In CMIP6 models, the AMOC gradually weakens up to 2100 and, independent of the used emission scenario (Weijer et al., 2020), no AMOC tipping is found. However, these models are thought to be biased towards a too stable AMOC (e.g. Cheng et al., 2018; Weijer et al., 2019), and a recent observation based study has indicated that the AMOC may tip between 2025 and 2095 (Ditlevsen & Ditlevsen, 2023).

The carbon cycle is also affected by climate change. In the ocean, the effect on the solubility pump is relatively straight forward: increased warming, and increased CO₂ concentrations, reduce ocean pH and the solubility of CO₂, which reduces the uptake capacity of the ocean (Sarmiento et al., 1998). The biological pump in Coupled Model Intercomparison Project 6 (CMIP6; Eyring et al., 2016) models is much more uncertain though (Henson et al., 2022; Wilson et al., 2022), especially given that the spread in NPP and Export Production (EP) has increased from CMIP5 to CMIP6 (Kwiatkowski et al., 2020; Tagliabue et al., 2021). The terrestrial biosphere is affected for example through increased primary production related to CO₂ fertilization (Zhu et al., 2022), but also increased respiration due to permafrost melt (Burke et al., 2020).

Studies looking at the combined effect of strong AMOC weakening and anthropogenic climate change on the future carbon cycle are limited. A projected AMOC weakening affects both the solubility and the biological carbon pumps (Liu et al., 2023), and generally leads to reduced uptake of (anthropogenic) carbon in the ocean (Obata, 2007; Zickfeld et al., 2008; Liu et al., 2023), which can be partially compensated for by the terrestrial biosphere (Zickfeld et al., 2008). However, the net effect has been found to be small due to competing effects (Swingedouw et al., 2007; Zickfeld et al., 2008). Though global effects might be weak, local effects can be quite strong. For example, a weakening of the AMOC can also result in a local reduction in primary productivity (Whitt & Jansen, 2020), changes in the plankton stock (Schmittner, 2005) and plankton composition (Boot et al., 2023a), which all can lead to reduced CO₂ uptake of the ocean (e.g. Yamamoto

et al., 2018; Boot et al., 2023a). These local changes related to an AMOC weakening are strongest in the Atlantic Ocean (Katavouta & Williams, 2021).

The novel aspect of this paper is that we consider the effect of AMOC weakening on the carbon cycle under climate change in a state-of-the-art global climate model, the Community Earth System Model v2 (CESM2; Danabasoglu et al., 2020), as explained in section 2. We use a strong freshwater forcing in the North Atlantic to artificially weaken the AMOC and consider two different emission scenarios, Shared Socioeconomic Pathways (SSPs), with low (SSP1-2.6) and high (SSP5-8.5) emissions (O'Neill et al., 2020). In the results of section 3 and the subsequent analysis, we focus on the mechanisms how a forced AMOC weakening affects atmospheric pCO₂ under climate change.

2 Method

In the CESM2 (Danabasoglu et al., 2020), the atmosphere is represented by the CAM6 model, the land by the CLM5 model (Lawrence et al., 2019), sea ice by the CICE model, ocean circulation by POP2 (Smith et al., 2010), and ocean biogeochemistry by MARBL (Long et al., 2021). The ocean models POP2 and MARBL are both run on a displaced Greenland pole grid at a nominal horizontal resolution of 1°, with 60 non-equidistant vertical levels. The ocean biogeochemical module MARBL is based on a NPZD-model, where four nutrients (N, P, Fe, and Si) together with light co-limit the production of three phytoplankton groups (diatoms, diazotrophs and small phytoplankton) which are grazed upon by one zooplankton group. The terrestrial carbon cycle is represented with CLM5. This module represents several surface processes such as biogeochemistry, ecology, human influences, biogeophysics and the hydrological cycle. As we use the default CESM2 version, there is no dynamic vegetation. For a complete overview of the CESM2 model and submodules we refer the reader to Danabasoglu et al. (2020) (CESM2), Long et al. (2021) (MARBL), and Lawrence et al. (2019) (CLM5).

We performed emission forced CESM2 simulations with two different emission scenarios, the low emission scenario SSP1-2.6 (126) and the high emission scenario SSP5-8.5 (585). For each emission scenario, a control (CTL) and a hosing (HOS) simulation were carried out. The CTL simulations were only forced with the greenhouse gas emissions, while the HOS simulations were forced with greenhouse gas emissions and an additional, artificial freshwater flux in the North Atlantic. This freshwater forcing is located in the North Atlantic Ocean over the latitudes 50°N - 70°N (Fig. S1), and is kept constant at a rate of 0.5 Sv over the entire simulation period. We will refer to the simulations by their simulation type (CTL or HOS) and the respective emission scenario (126 or 585), e.g. as CTL-126 and HOS-585. All simulations are run from year 2015 to year 2100 and are initialized by values of the NCAR CMIP6 emission driven historical simulation (Danabasoglu, 2019). The used model output is based on monthly means, and line plots are smoothed with a 5 year running mean. When looking at the difference between the HOS and CTL simulations, we subtract the CTL simulations from the HOS simulations.

3 Results

3.1 Climate reponse

In CTL-126, an increase in atmospheric CO₂ concentration from 400 ppm to 467 ppm in the 2050s is found, after which the concentration decreases to 432 ppm in 2100 (Fig. 1c). This is accompanied by an increase in global mean surface temperature (GMST) of 1 °C (Fig. 1b), and an AMOC decrease from 17 Sv in 2015 to 9 Sv in 2100 (Fig. 1a). The weakening of the AMOC results in a cooling of the North Atlantic Ocean, while the rest of the Earth warms with largest temperature increases found near the poles (Fig. 2a, b) as a response to the increase in greenhouse gas concentrations. In the water cy-

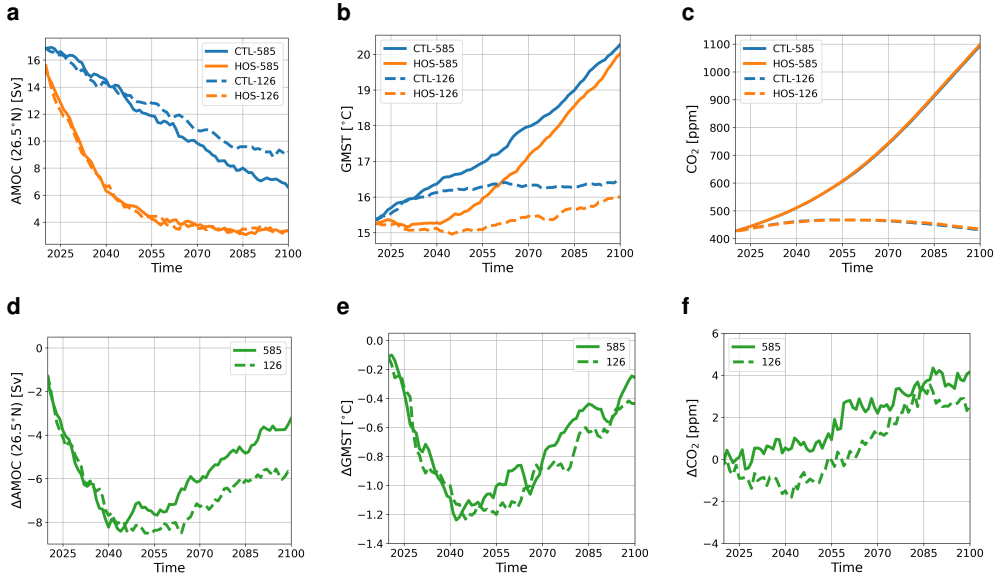


Figure 1. (a) AMOC strength at 26.5°N in Sv. (b) GMST in °C. (c) Atmospheric CO₂ concentration in ppm. In (a-c) blue lines represent the control (CTL) simulations, and orange lines the HOS simulations. (d-f) as in (a-c) but for the difference between the HOS simulations and the control simulations. In all subplots dashed lines represent SSP1-2.6 (126) and solid lines SSP5-8.5 (585).

165 cle we see a southward shift of the Pacific InterTropical Convergence Zone (ITCZ) of a
 166 few degrees (Fig. S2a, b). Furthermore, wind fields in the Northern Hemisphere show
 167 a small weakening, whereas in the Southern Hemisphere the winds intensify (Fig. S3a,
 168 b).

169 In CTL-585, the emissions increase the atmospheric CO₂ concentration from 400 ppm
 170 to 1094 ppm in 2100 (Fig. 1c) which results in a GMST warming of 5 °C (Fig. 1b). The
 171 AMOC weakens from 17 Sv to 7 Sv (Fig. 1a), which leads to a region without warm-
 172 ing in the North Atlantic, whereas we see strong warming everywhere else (Fig. 2d, e).
 173 There is a strong southward shift of the ITCZ in the Pacific and a moderate shift in the
 174 Atlantic Ocean (Fig. S2d, e). The changes in the wind field show similar patterns as CTL-
 175 126 but with a larger amplitude (Fig. S3d, e).

176 The net effect of the AMOC weakening (i.e. HOS minus CTL) is shown in Fig. 1def.
 177 In the year 2100, atmospheric CO₂ concentrations are 2.6 ppm and 4.2 ppm higher in
 178 HOS-126 and HOS-585 compared to their respective CTL simulations. In both HOS sim-
 179 ulations the AMOC quickly weakens from 17 Sv in 2015 to 6 Sv in 2045 after which the
 180 AMOC weakening starts to level off until the AMOC is weaker than 4 Sv in 2100 (Fig.
 181 1d). Due to the AMOC weakening we observe a relative cooling of (locally) more than
 182 3 °C in the Northern Hemisphere and warming in the Southern Hemisphere (Fig. 2c,
 183 f) (i.e. the bipolar seesaw). The cooling in the Northern Hemisphere results into an in-
 184 crease in sea-ice cover of the Arctic Ocean (Fig. S4), which for HOS-126 persists through-
 185 out the entire simulation period. The AMOC weakening also results into a stronger south-
 186 ward shift of the ITCZ in both the Pacific and Atlantic Ocean (Fig. S2c, f), and winds
 187 are relatively intensified in the Northern Hemisphere and weakened in the Southern Hemis-
 188 sphere (Fig. S3c, f), with a stronger response in SSP5-8.5.

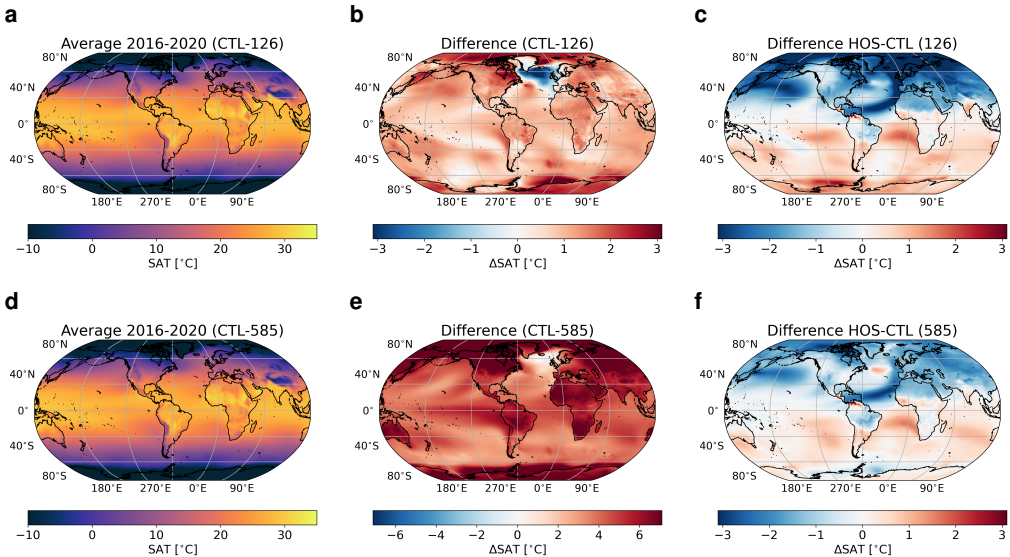


Figure 2. Results for Surface Air Temperature (SAT) in $^{\circ}\text{C}$. The top row (a-c) is for SSP1-2.6, and the bottom row (d-f) for SSP5-8.5. The left column (a, d) represents the average over 2016-2020 in the control simulations. The middle row (b, e) represents the difference between the average of 2096-2100 and 2016-2020 for the control simulations. The right row (c, f) represents the difference between the HOS and CTL simulations averaged over 2096-2100. Note the different scaling between b and e.

189

3.2 Marine carbon cycle response

190
191
192
193
194
195
196
197
198
199
200
201

In CTL-126 we see that, integrated over the entire simulation period, there are regions in the ocean with net carbon uptake, and net carbon outgassing (Fig. 3a). The Southern Ocean between 45°S and 60°S , and the equatorial Pacific Ocean, are regions of carbon release from the ocean to the atmosphere. The region of strongest outgassing in the Pacific is located in the upwelling regions on the eastern side of the basin. Carbon uptake generally occurs in the rest of the ocean with the strongest uptake located in the Sea of Japan and the high latitude North Atlantic Ocean. Looking at the development over time (Fig. 4a, b) we see a negative trend over almost the entire ocean, meaning regions which take up carbon in the beginning of the simulation have lower uptake at the end, and regions which emit carbon in 2015 emit more carbon at the end of the simulation. Some regions, e.g. in the Southern Ocean, shift from a carbon uptake region to a region of outgassing.

202
203
204
205
206
207
208
209
210
211
212

In CTL-585, also integrated over the simulation period, only the eastern equatorial Pacific shows strong outgassing (Fig. 3d). In the other equatorial basins, there are also some small patches that show net outgassing, but the rest of the ocean shows net carbon uptake. Except for the high latitude North Atlantic Ocean and some small other regions, we see a positive trend (Fig. 4d, e), meaning that regions that take up carbon in the beginning, take up more carbon at the end of the simulation, and regions which show outgassing in the beginning show either reduced outgassing or go from being a region of outgassing to a region of CO_2 uptake. A remarkable region is the high latitude North Atlantic Ocean where the flux from the atmosphere into the ocean strongly decreases while atmospheric pCO_2 almost triples. Integrated over time, the spatial pattern of regions that see increased or decreased exchange with the atmosphere is very sim-

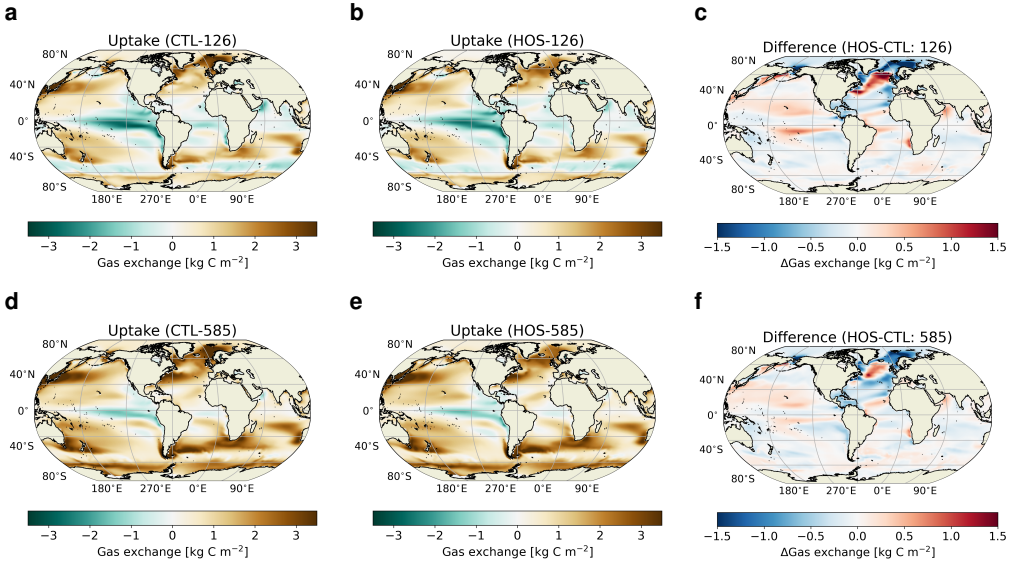


Figure 3. Results for the oceanic CO_2 uptake integrated over the entire simulation period in kg C m^{-2} . The top row (a-c) represents SSP1-2.6 and the bottom row (d-f) represents SSP5-8.5. The left column (a, d) represents the uptake in the control simulations, the middle column (b, e) the uptake in the HOS simulations, and the right column (c, f) the difference between the HOS and CTL simulations. In a, b, d, and e positive values (brown colors) represent net uptake, and negative values (blue colors) represent net outgassing.

ilar for SSP1-2.6 as for SSP5-8.5 (Fig. 3c, f). In total, the ocean takes up 7.4 PgC less due to the AMOC weakening in SSP1-2.6 and 15.6 PgC less in SSP5-8.5 (Fig. 5a, d).

Even though the climate system changes a lot due to the AMOC weakening, the CO_2 uptake of the ocean does not change a lot because of compensating effects. To obtain a better understanding of the mechanisms behind the reduced uptake, we have divided the ocean into 5 basins: the Arctic (north of 66°N), the Southern (south of 35°S), the Atlantic, Pacific and Indian Ocean (Fig. 5b, e). In the response (i.e. HOS-CTL), for both emission scenarios, all basins show the same sign, i.e. more uptake or less uptake due to the AMOC weakening.

In both emission scenarios the Arctic Ocean shows a decreased uptake (-6.0 PgC in SSP1-2.6 and -4.4 PgC in SSP5-8.5), which can be explained by looking at the sea-ice cover (Fig. S4). The cooling in the Northern Hemisphere following the AMOC weakening in the HOS simulations, increases the sea-ice cover. The increase in sea-ice cover has two effects on the uptake of CO_2 : (1) it reduces the ocean area available for exchange with the atmosphere; and (2) it increases light limitation and thereby reduces net primary production (NPP; Fig. S6) and the carbon export to the subsurface ocean. In SSP5-8.5 most of the sea ice still disappears due to the strong warming, but in SSP1-2.6 most of the sea ice persists throughout the simulation period, which explains why the Arctic Ocean in SSP1-2.6 responds stronger compared to SSP5-8.5. We also find this effect in the sea-ice covered regions in the North Atlantic (e.g. the Labrador Sea).

The Pacific Ocean takes up more carbon in the HOS than in the CTL simulations (+4.9 PgC in SSP1-2.6 and +1.7 PgC in SSP5-8.5). To analyze what is happening in the Pacific, we considered three different regions: (1) the North Pacific (20°N - 66°N), the Equatorial Pacific (20°N - 10°S), and the South Pacific (10°S - 35°S). In the North Pacific,

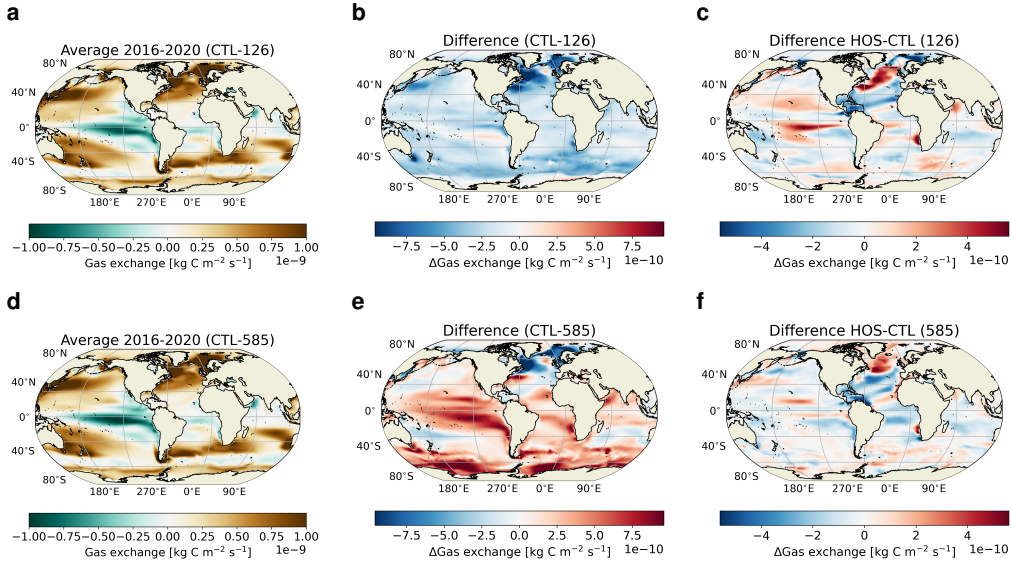


Figure 4. Results for oceanic CO₂ uptake in kg C m⁻² s⁻¹. Panels represent the same as in Fig. 2. Positive values (brown colors) in a and d represent uptake by the ocean and negative values (blue colors) represent outgassing.

the relative cooling of the surface ocean (Fig. S7) results in an increase of solubility of CO₂ driving increased uptake (Fig. 3e, f). A similar, but opposite, response is seen in the South Pacific. Here the surface ocean becomes relatively warmer inhibiting the uptake of CO₂. The equatorial Pacific is characterized by a band with reduced uptake and one with increased uptake. This can be related to the stronger southward shift of the ITCZ in the Pacific in HOS compared to the CTL (Fig. S2). Due to this shift, the dilutive fluxes related to net precipitation shift southward, causing relative increases of salinity in the northern section due to reduced precipitation, and relative decreases due to increased precipitation in the southern section (Fig. S8). This, in turn, also affects the stratification in these regions with a weakening in the north and a strengthening in the south (Fig. S9). These changes affect the solubility of CO₂ in the equatorial regions causing decreased uptake in the northern section and increased uptake in the southern section.

We find the largest difference in carbon uptake (-2.0 PgC in SSP1-2.6 and -9.3 PgC in SSP5-8.5) in the Atlantic. The regions with sea ice show similar behavior as the Arctic Ocean with decreased uptake related to a larger sea-ice cover in the HOS simulations. In the ice-free subpolar region, an increase in uptake is observed which is associated to decreases in sea surface salinity (SSS; Fig. S8) due to the applied freshwater forcing in this region which promotes the uptake of CO₂. In the subtropical region we generally see a decrease in uptake. To explain this we consider several variables, i.e. SST (Fig. S7), SSS (Fig. S8), DIC (Fig. S12), Alk (Fig. S13) and NPP (Fig. S6), which all show a relative decrease in this region. The net effect of the changes in these variables is a reduction in pH (Fig. S16) and reduced uptake capacity of the ocean. In the Canary Upwelling System and along the North Equatorial Current we do see an increase in NPP (Fig. S6), due to increased nutrient concentrations (Fig. S11) related to increased upwelling of nutrients (Fig. S10 and S15). In the region of the North Equatorial Current this leads to increased uptake of the ocean, and only in SSP5-8.5 also in the Canary Upwelling System. Outside the North Atlantic, large responses are seen in the equatorial region and the Benguela Upwelling System which are characterized by reduced upwelling (Fig. S10),

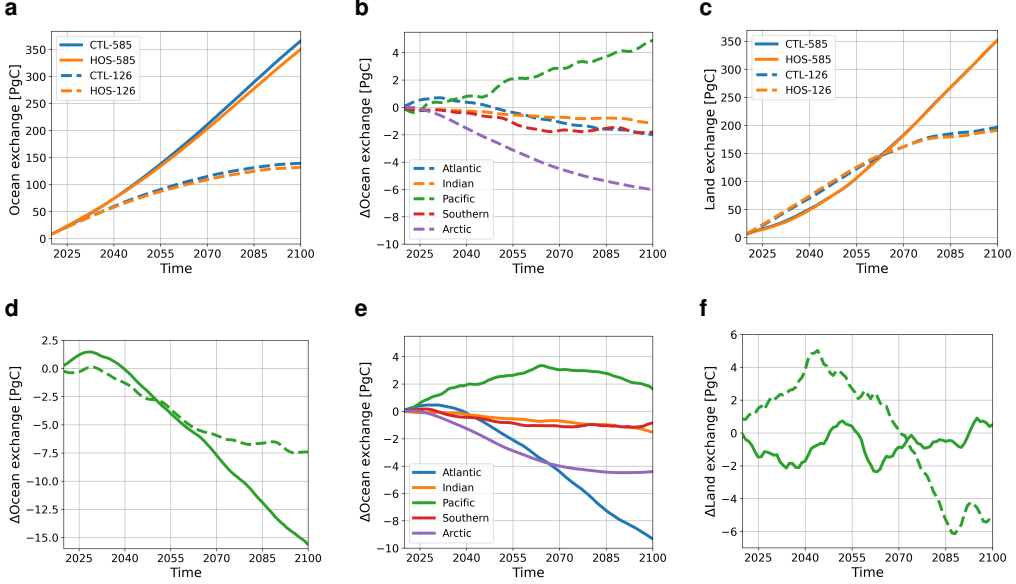


Figure 5. (a) Cumulative uptake of CO₂ in the ocean from 2016 onward in PgC. (b) Difference in the cumulative oceanic CO₂ uptake between the HOS and CTL simulations in SSP1-2.6 for different ocean basins. (c) As (a) but for the land. (d) The difference in the cumulative oceanic CO₂ uptake between the HOS and CTL simulations. (e) As in (b) but for SSP5-8.5. (f) As in (d) but for the land. In a and c blue lines represent the control simulations, and the orange lines the HOS simulations. In all subplots dashed lines represent SSP1-2.6 and solid lines SSP5-8.5. Negative values in b, d-f represent reduced uptake in the HOS simulations compared to the CTL simulations.

promoting additional uptake of CO₂ in the ocean. In the Atlantic Ocean, we find that DIC (Fig. 6) and nutrient (Fig. 7) concentrations decrease in the surface ocean due to the weakening of the AMOC and increase in the deep ocean. The reduction in DIC clearly shows the reduced uptake capacity of the ocean, and the reduction in PO₄ also explains the decrease in NPP (Fig. S6) observed in the Atlantic basin.

The Indian Ocean has a relatively weak response and is very similar for both emission scenarios with a small decrease in uptake (-1.2 PgC in SSP1-2.6 and -1.5 PgC in SSP5-8.5). This is related to the relatively warmer SSTs in the HOS simulations (Fig. S7). The Southern Ocean also has a small decrease in uptake, with a larger decrease in SSP1-2.6 (-1.8 PgC compared to -0.9 PgC in SSP5-8.5). This larger decrease can be explained by the fact that the sea-ice cover is larger in SSP1-2.6 compared to SSP5-8.5 (Fig. S5).

3.3 Terrestrial carbon cycle response

In CTL-126, the terrestrial biosphere, integrated over the entire simulation period, shows a net uptake of CO₂ in most regions (Fig. 8a). The Net Biosphere Production (NBP) maxima are located on the equator for the tropical rainforests, the boreal forests in the high latitude Northern Hemisphere, and the eastern United States and China. The few locations that show net emission of CO₂ are very local and present in the high latitude Northern Hemisphere, the Tibetan Plateau, South East Asia and South America. If we look at the development over time (Fig. 9a, b) we see that the tropical rainforests have

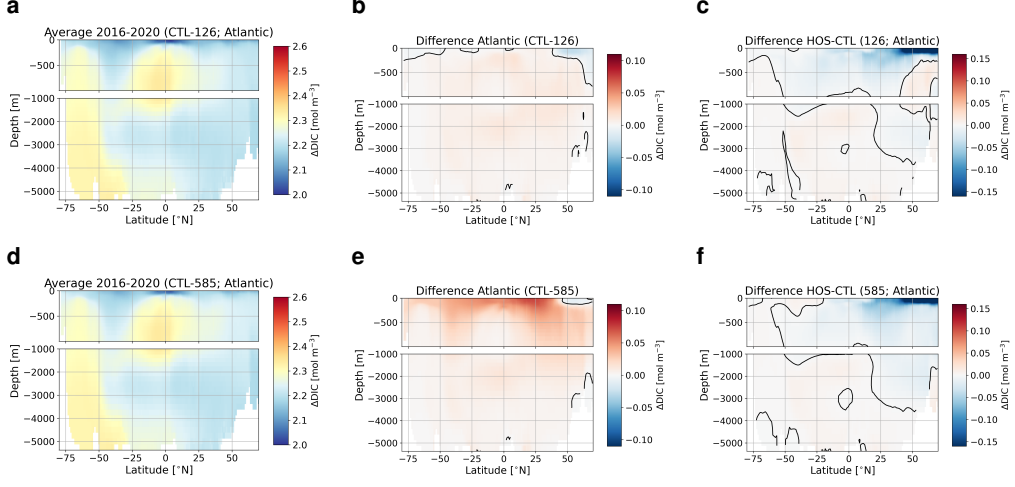


Figure 6. Results for zonally averaged DIC concentrations in the Atlantic basin in mol m^{-3} . Panels represent the same as in Fig. 2. Black contour lines in b, c, e and f represent the 0 mol m^{-3} contour. Note the different scaling of the surface ocean (top 1000 m) compared to the deep ocean.

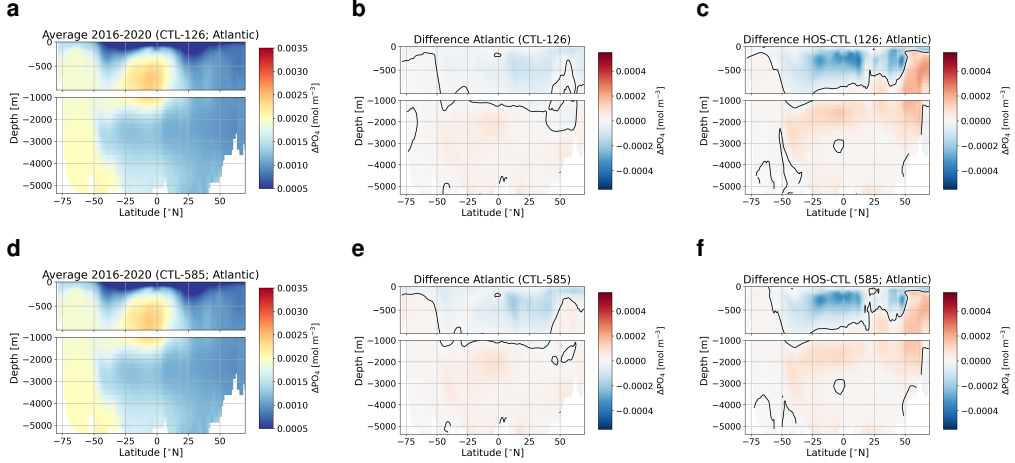


Figure 7. Results for zonally averaged PO₄ concentrations in the Atlantic basin in mol m^{-3} . Panels represent the same as in Fig. 2. Black contour lines in b, c, e and f represent the 0 mol m^{-3} contour. Note the different scaling of the surface ocean (top 1000 m) compared to the deep ocean.

286 a lower NBP at the end of the simulation. There are some regions that have a higher
287 NBP in 2100, e.g. the boreal forests in Scandinavia.

288 The response in CTL-585 is very similar to CTL-126 with respect to the spatial
 289 pattern, except in central Africa (Fig. 8d). However, the amplitude of the response is
 290 much larger due to the CO₂ fertilization effect. Especially the tropical rainforests, but
 291 also the boreal forests, show more carbon uptake compared to CTL-126. The same is
 292 also true for regions that emit carbon, i.e., the region in the high latitude Northern Hemis-
 293 phere that emits carbon is larger, and the amount of carbon emitted is also higher. The
 294 main difference with respect to CTL-126 is a region in the Congo basin which emits CO₂
 295 in CTL-585 whereas in CTL-126 it is a region of relatively strong uptake, which is pos-
 296 sibly related to increased wildfire activity in this region in SSP5-8.5 (Fig. S17). When
 297 we look at the development over time (Fig. 9d, e) we find a completely different pattern
 298 in CTL-585 compared with CTL-126. The tropical rainforests show an increase in NBP
 299 related to the CO₂ fertilization effect whereas northern Siberia shows a decrease related
 300 to increased respiration due to permafrost melt (Fig. S19 and S20).

301 Integrated globally the terrestrial biosphere takes up 5.3 PgC less in SSP1-2.6 and
 302 0.5 PgC more in SSP5-8.5 (Fig. 5) in the HOS simulations compared to the CTL sim-
 303 ulations. However, looking at spatial patterns of the cumulative uptake, we see a very
 304 similar response to the AMOC weakening (HOS-CTL) for both emission scenarios (Fig.
 305 8c, f). In both emission scenarios we find that the increased southward shift in the ITCZ
 306 in the HOS simulations lead to decreased NBP in central America, and increased NBP
 307 in Southern America. A similar shift can be seen in Africa, but with a smaller latitu-
 308 dinal shift and amplitude. The shift and amplitude are slightly stronger in SSP1-2.6. The
 309 boreal forests become relatively lower in NBP in the HOS simulations with a larger am-
 310 plitude in SSP1-2.6. This is because in SSP1-2.6, the forests have lower Gross Primary
 311 Production (GPP; Fig. S18) over the course of the century which can be related to the
 312 relative cooling in the Northern Hemisphere seen in the HOS simulations (Fig. S8). This
 313 relative cooling is stronger in SSP1-2.6, related to the increased sea-ice cover and there-
 314 fore higher albedo in the Arctic. Another effect of the Northern Hemispheric cooling is
 315 an increase in NBP in the permafrost regions in Siberia and North America in the HOS
 316 simulations. The cooling reduces permafrost melt (Fig. S19) and therefore reduces soil
 317 respiration (Fig. S20), with a larger amplitude in Siberia for SSP5-8.5.

318 3.4 Total response

319 In total we see an increase of atmospheric CO₂ concentration of 2.6 and 4.2 ppm
 320 in 2100 in SSP1-2.6 and SSP5-8.5 due to the AMOC weakening (HOS-CTL). In SSP1-
 321 2.6 this response is caused partly due to reduced uptake of the ocean and partly due to
 322 reduced uptake of the land. In SSP5-8.5 it is completely driven by the ocean as the glob-
 323 ally integrated uptake over the land is approximately the same in CTL-585 as in HOS-
 324 585. Eventually the AMOC strength in 2100 has decreased by 5.8 and 3.2 Sv in the HOS
 325 simulations compared to the CTL simulations. Under the assumption of linearity, this
 326 results in a positive feedback strength of 0.44 ppm Sv⁻¹ and 1.3 ppm Sv⁻¹ for SSP1-
 327 2.6 and SSP5-8.5 respectively. This can be considered a positive feedback since increased
 328 CO₂ concentrations in future climates are generally associated with a weakening of the
 329 AMOC (e.g. Weijer et al., 2020). This AMOC-pCO₂ feedback is small on the global scale,
 330 due to competing effects but locally large changes in carbon uptake can occur.

331 Fig. 10 gives an overview of the most important climate changes and how the ma-
 332 rine and terrestrial respond to these changes. In Fig. 10c, d the difference between SSP1-
 333 2.6 and 5-8.5 is highlighted. In the terrestrial biosphere the prime effect of the AMOC
 334 weakening is the southward shift of the GPP maxima in the tropical rainforests (Fig. S18).
 335 Though this could potentially have beneficial effects for the southern regions, it could
 336 have detrimental effects for the northern regions (e.g. the Sahel region) and could for
 337 example increase the latitudinal extent of the Sahara desert. This shift, caused by a shift
 338 in precipitation (Fig. S2), also has effects for the probability of wildfires (Fig. S17), which
 339 can increase in regions with reduced precipitation. We cannot conclude whether the AMOC

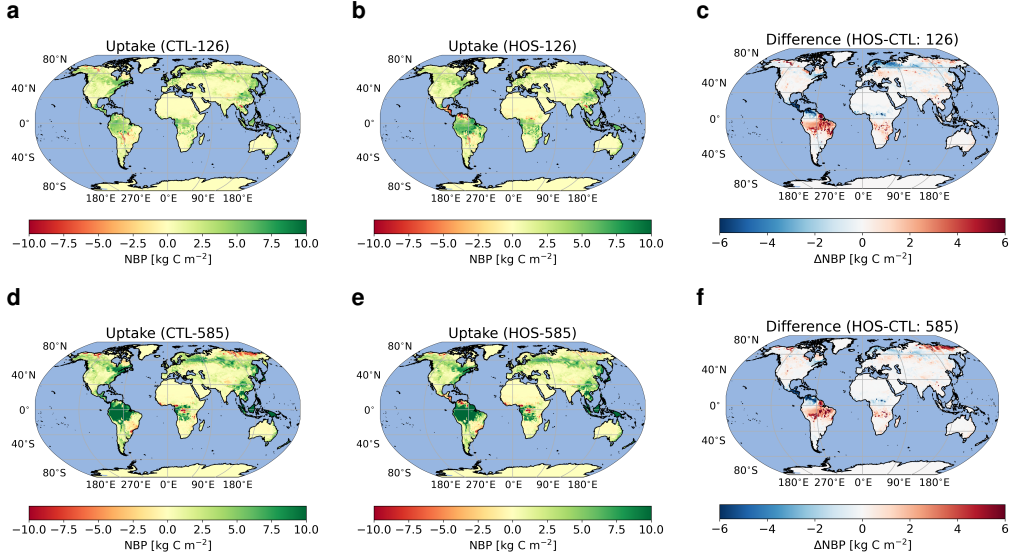


Figure 8. Results for the CO₂ exchange with the land integrated over the entire simulation period in kg C m⁻². The top row (a-c) represents SSP1-2.6 and the bottom row (d-f) represents SSP5-8.5. The left column (a, d) represents the uptake in the control simulations, the middle column (b, e) the uptake in the HOS simulations, and the right column (c, f) the difference between the HOS and CTL simulations. In a, b, d, and e green colors represent net CO₂ uptake by the land, and red colors represent net emissions into the atmosphere.

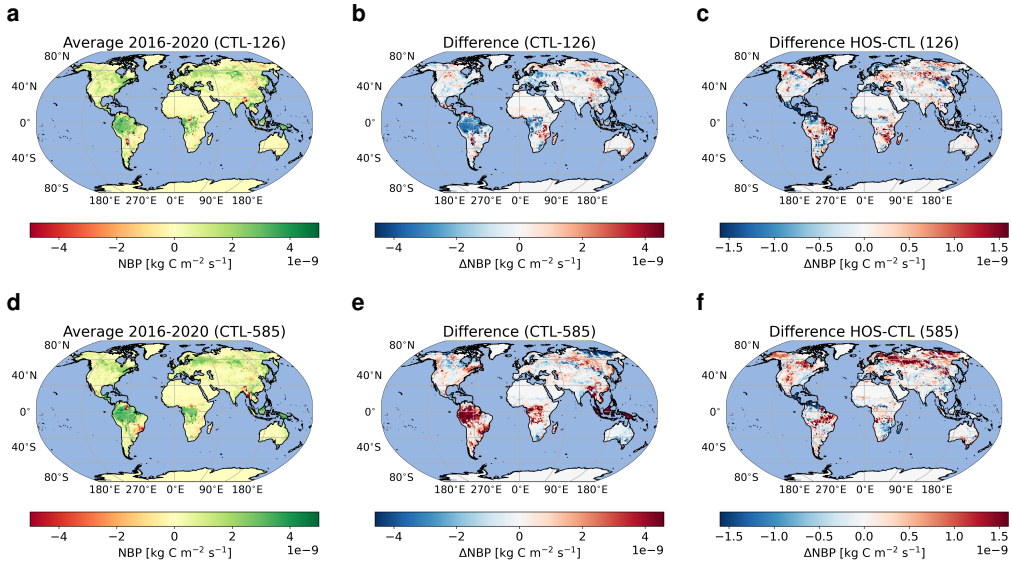


Figure 9. Results for Net Biosphere Production (NBP) in kg C m⁻² s⁻¹. Panels represent the same as in Fig. 2. Green colors represent uptake of CO₂ into the land and red colors represent emission of CO₂ to the atmosphere.

weakening would result into a collapse of the Amazonian rainforests or an increase in the Sahara desert since the model is used without a dynamic vegetation model. In the ocean,

a decrease in NPP (Fig. S6) and surface nutrient concentrations (Fig. S11) occurs. The changes in NPP can have effects on the entire food web and thereby have a negative impact on ecosystems and ecosystem functions. If the trend of the surface ocean becoming more depleted of nutrients (Fig. 7) continues, this might drive a large decline in NPP for the coming centuries. Another important effect of the AMOC weakening is increased ocean acidification (i.e. a decrease in pH; Fig. S16). Lower pH values increase the stress on calcifying organisms and reduces the uptake capacity of the ocean, which might increase the AMOC-pCO₂ feedback strength on longer timescales.

In many climate and carbon cycle variables we see a similar response in spatial pattern, but sometimes with a slightly different amplitude (Fig. 10c, d). In the terrestrial biosphere, the main differences are seen in the boreal forests in Scandinavia and Russia (box 1 in Fig. 10), and in the Siberian permafrost regions (box 2). The difference in the boreal forests can be explained by looking at the temperature differences between the HOS and CTL simulations. In SSP1-2.6, the northern hemisphere cools more, which causes increased GPP reduction in the boreal forests. For the permafrost region we find a stronger response in SSP5-8.5, because in SSP1-2.6 there is not much permafrost melt in the CTL simulation; therefore the additional cooling in the HOS simulation does not have a large effect on the permafrost melt. In the ocean, we find the largest changes in the subpolar North Atlantic and the Arctic sea-ice regions (boxes 7 and 8 in Fig. 10). In the subpolar region there is a relatively stronger decrease in SSS and SST (Fig. S7 and S8) in SSP1-2.6 compared to 5-8.5 leading to a larger increase in solubility of CO₂ and therefore more uptake. Because of the increased cooling, and lower background temperatures in SSP1-2.6, sea-ice cover does not diminish over the simulation whereas in SSP5-8.5 we see in both simulations a strong reduction in sea-ice cover (Fig. S4). This is the reason why we see a stronger reduction in the Arctic in SSP1-2.6.

4 Summary and discussion

In this study, we have investigated the carbon cycle response to a weakening of the Atlantic Meridional Overturning Circulation (AMOC) under climate change scenarios. We did this by forcing a state-of-the-art Earth System Model, the Community Earth System Model v2 (CESM2), on a nominal 1° resolution with emissions from two different SSP scenarios (SSP1-2.6 and SSP5-8.5) and an additional freshwater flux in the North Atlantic to artificially decrease the AMOC. To our knowledge, this is the first study that utilizes a model of this high complexity with a horizontal resolution of 1° to study the effects of an AMOC weakening on the carbon cycle. We find a positive feedback in both emission scenarios of 0.44 ppm Sv⁻¹ and 1.3 ppm Sv⁻¹ for SSP1-2.6 and SSP5-8.5, respectively. The response in SSP1-2.6 is driven by both the land and ocean carbon reservoirs, whereas in SSP5-8.5 it is driven solely by the ocean. The response is small, being the effect of many compensating effects over both the land and the ocean. Looking at regional response patterns, both emission scenarios show similar behavior in many climate and carbon cycle variables. In absolute numbers, the response is stronger in SSP5-8.5, but when the high CO₂ concentrations are taken into account, the relative response is actually weaker in SSP5-8.5 compared to SSP1-2.6.

Our simulations show the climate response to an AMOC weakening, such as a southward shift of the ITCZ and the bipolar seesaw, similar to many previous studies (Obata, 2007; Zickfeld et al., 2008; Orihuela-Pinto et al., 2022). The AMOC weakening in our simulations follows a very similar trajectory as in Orihuela-Pinto et al. (2022), which used an older version of CESM (i.e. v1.2) under pre-industrial boundary conditions. In our study, the AMOC weakening results in a small increase in atmospheric CO₂ concentrations. This small effect, especially on the multi-decadal to centennial timescales assessed here, was also found in more idealized models (e.g. Zickfeld et al., 2008; Nielsen et al., 2019; Gottschalk et al., 2019), but as described in Gottschalk et al. (2019) the relative response of the ocean and land reservoirs are dependent on climatic boundary conditions

and the used model. Here, we have used a member of the newest generation of Earth System Models with a relatively high spatial resolution (i.e. nominal $1^\circ \times 1^\circ$ ocean grid). When considering studies with induced AMOC weakening we find, integrated over the entire ocean, a similar response as in Zickfeld et al. (2008), and spatially as in Obata (2007), though local differences remain which can be attributed to the use of a higher resolution, and a more complex model in our study. It is also possible to collapse the AMOC without an additional freshwater forcing. In Nielsen et al. (2019) they used such an alternative method under Pleistocene conditions, which resulted in a much slower response in the ocean compared to our simulations. The response of the terrestrial biosphere, especially the changes related to the southward shift of the ITCZ, is also similar to that of previous studies using static vegetation (e.g. Obata, 2007; Nielsen et al., 2019). In Köhler et al. (2005) a dynamic vegetation model is used, and they show that an AMOC collapse affects vegetation type. This leads to reduced carbon storage in the high latitudes and increased carbon storage in the Northern Hemisphere midlatitudes. This dynamic behavior is not captured in our simulations and unfortunately, it is not possible to assess what the effect of dynamic vegetation would be based on Köhler et al. (2005) since they consider Pleistocene conditions.

The result that the pattern of the carbon cycle response to an AMOC weakening is independent of the cumulative CO₂ emissions on multi-decadal to centennial timescales has been shown before. In Zickfeld et al. (2008), for example, the marine carbon cycle remains independent on the used emission scenario for the first 200 years of their simulation, and for the terrestrial carbon cycle this is 150 years. After this period the different emissions start to diverge, though the qualitative behavior remains similar. In our simulations, globally integrated variables show little change as a response to the AMOC weakening. However, on regional scales the effects of an AMOC weakening can be large, e.g. SATs can decrease or increase by more than 3 °C locally (Fig. 2) and some regions become much drier and other see a large increase in precipitation (Fig. S2). These changing climate conditions, on top of already greenhouse gas driven climate change, require climate adaptation which might be difficult to achieve in such a short time frame (i.e. decades). The climate changes associated to an AMOC weakening also cause changes in the carbon cycle. Such changes can increase, for example, desertification and reduce (but also increase) crop yields. This may lead locally to increased food stress, potentially leading to more frequent and more severe famines. The changes in the ocean can lead to more frequent marine heatwaves in the Southern Hemisphere due to the warming, and reduced (global) NPP due to changing nutrient distributions, which might impact food web dynamics and ecosystem function. However, due to the cooling effect of the bipolar seesaw we would also expect a (relative) reduction in marine heatwaves in the Northern Hemisphere. These effects show that an AMOC collapse can have local effects that have a beneficiary impact or a detrimental impact on the terrestrial and marine biospheres.

Interestingly, the relative effects on multi-decadal timescales are independent to the (cumulative) greenhouse gas emissions. This means that the uncertainty around the effects of a possible AMOC collapse or weakening is not related to past emissions. However, in a future climate without AMOC weakening, emissions do have an influence on when the AMOC might collapse. Furthermore, the small positive feedback found in this study might make the AMOC more likely to tip earlier. Even though on these timescales the relative effects are not dependent on the greenhouse gas emissions, this might be different on intermediate (multi-centennial to millennial) timescales. Because the ocean circulation is associated with timescales on the intermediate timescales, we can expect the most important effects to occur in this time frame. We find, for example, that the surface ocean is becoming more depleted of nutrients (Fig. 7), which might depress NPP for centuries.

446 Other long term effects that might be relevant are tipping cascades (e.g. Dekker
 447 et al., 2018), meaning that a collapse of the AMOC could set off an other tipping ele-
 448 ment in the Earth System. In our simulations, we find decreasing temperatures in the
 449 Northern Hemisphere due to the AMOC weakening, which reduces the probability of tip-
 450 ping for example melting of the Greenland Ice Sheet, Arctic sea ice, and Northern Hemis-
 451 pheric permafrost. However, due to the bipolar seesaw, the Southern Hemisphere be-
 452 comes warmer, which might increase the probability of tipping the Antarctic Ice Sheets.
 453 Another tipping point connected to the AMOC is the die off of the Amazonian rainfor-
 454 est. Because we do not use a dynamic vegetation model in this study, we cannot inves-
 455 tigate whether the AMOC weakening in our simulations would lead to such a die off.

456 By using a low and a high emission scenario we have tried to cover uncertainties
 457 regarding future emissions. However, we have only used one Earth System Model, which
 458 means that the results presented here could be model dependent. Especially ocean pro-
 459 ductivity shows large spread in the CMIP6 ensemble, which can influence the uptake ca-
 460 pacity of the ocean. Another bias in Earth System Models is a too stable AMOC, mean-
 461 ing we need a large freshwater flux in the North Atlantic Ocean to weaken the AMOC.
 462 This flux is generally too high to represent for example Greenland Ice Sheet melt, but
 463 necessary to achieve a weakened AMOC. This large freshwater flux also leads to fresh-
 464 ening of the surface ocean in the subpolar gyre which influences the carbonate chemistry
 465 and carbon uptake capacity unrealistically. We have not taken this effect into account
 466 explicitly, but it could potentially result in reduced uptake capacity of the ocean, and
 467 therefore more CO₂ in the atmosphere, increasing the feedback strength.

468 Finally, we have shown in a relatively high resolution, state-of-the-art Earth Sys-
 469 tem Model, that the spatial pattern of the carbon cycle response to an AMOC weaken-
 470 ing is not dependent on cumulative CO₂ emissions. As a follow up study it would be in-
 471 teresting to see what happens on multi-centennial and longer timescales, and what the
 472 pCO₂ response would be under an AMOC recovery. Though not analyzed thoroughly,
 473 NPP in the ocean shows large decreases due to the AMOC weakening. This could ef-
 474 fect food web dynamics in the ocean with possible (detrimental) changes in fishery yields,
 475 food securities and income. These ecosystem and socio-economic effects are worth in-
 476 vestigating, to see how a change in the climate system cascades through ecosystems to
 477 socio-economic systems.

478 Appendix A Open Science

479 Yearly output for the most important variables, data necessary to replicate the fig-
 480 ures, and the scripts used for creating the figures can be downloaded from <https://doi.org/10.5281/zenodo.8376701> (Boot et al., 2023b).

482 Acknowledgments

483 This study has been supported by the Netherlands Earth System Science Centre (NESSC),
 484 which is financially supported by the Ministry of Education, Culture and Science (OCW;
 485 grant no. 024.002.001). The authors want to thank Michael Kliphuis (IMAU, Utrecht
 486 University) for performing the CESM2 simulations, which were performed at SURF-
 487 sara in Amsterdam on the Dutch Supercomputer Snellius within NWO-SURF project
 488 17239.

489 References

- 490 Behrenfeld, M. J., O'Malley, R. T., Siegel, D. A., McClain, C. R., Sarmiento, J. L.,
 491 Feldman, G. C., ... Boss, E. S. (2006). Climate-driven trends in contem-
 492 porary ocean productivity. *Nature*, 444(7120), 752–755. Retrieved from
 493 <https://doi.org/10.1038/nature05317> doi: 10.1038/nature05317

- 494 Boot, A., von der Heydt, A. S., & Dijkstra, H. A. (2022). Effect of the At-
 495 lantic Meridional Overturning Circulation on atmospheric $p\text{CO}_2$
 496 variations. *Earth System Dynamics*, 13(3), 1041–1058. Retrieved from
 497 <https://esd.copernicus.org/articles/13/1041/2022/> doi: 10.5194/
 498 esd-13-1041-2022
- 499 Boot, A., von der Heydt, A. S., & Dijkstra, H. A. (2023a). Effect of Plankton
 500 Composition Shifts in the North Atlantic on Atmospheric pCO₂. *Geophys-
 501 ical Research Letters*, 50(2), e2022GL100230. Retrieved from <https://agupubs.onlinelibrary.wiley.com/doi/abs/10.1029/2022GL100230> doi:
 503 <https://doi.org/10.1029/2022GL100230>
- 504 Boot, A., von der Heydt, A. S., & Dijkstra, H. A. (2023b, September). *GBC_2023:*
 505 *v1.1_25_09_23 (v1.1)*. [dataset]. Zenodo. doi: 10.5281/zenodo.8376701
- 506 Buckley, M. W., & Marshall, J. (2016, mar). Observations, inferences, and mecha-
 507 nisms of the Atlantic Meridional Overturning Circulation: A review. *Reviews
 508 of Geophysics*, 54(1), 5–63. Retrieved from <https://doi.org/10.1002/2015RG000493> doi: <https://doi.org/10.1002/2015RG000493>
- 509 Burke, E. J., Zhang, Y., & Krinner, G. (2020). Evaluating permafrost physics
 510 in the Coupled Model Intercomparison Project 6 (CMIP6) models and their
 511 sensitivity to climate change. *The Cryosphere*, 14(9), 3155–3174. Re-
 512 tried from <https://tc.copernicus.org/articles/14/3155/2020/> doi:
 513 [10.5194/tc-14-3155-2020](https://doi.org/10.5194/tc-14-3155-2020)
- 514 Caesar, L., Rahmstorf, S., Robinson, A., Feulner, G., & Saba, V. (2018). Ob-
 515 served fingerprint of a weakening Atlantic Ocean overturning circulation.
 516 *Nature*, 556(7700), 191–196. Retrieved from <https://doi.org/10.1038/s41586-018-0006-5> doi: 10.1038/s41586-018-0006-5
- 517 Cheng, W., Weijer, W., Kim, W. M., Danabasoglu, G., Yeager, S. G., Gent,
 518 P. R., ... Zhang, J. (2018). Can the Salt-Advection Feedback Be De-
 519 tected in Internal Variability of the Atlantic Meridional Overturning Circu-
 520 lation? *Journal of Climate*, 31(16), 6649–6667. Retrieved from <https://journals.ametsoc.org/view/journals/clim/31/16/jcli-d-17-0825.1.xml>
 521 doi: <https://doi.org/10.1175/JCLI-D-17-0825.1>
- 522 Cuffey, K. M., & Clow, G. D. (1997, nov). Temperature, accumulation, and ice
 523 sheet elevation in central Greenland through the last deglacial transition.
 524 *Journal of Geophysical Research: Oceans*, 102(C12), 26383–26396. Retrieved
 525 from <https://doi.org/10.1029/96JC03981> doi: <https://doi.org/10.1029/96JC03981>
- 526 Danabasoglu, G. (2019). *NCAR CESM2 model output prepared for CMIP6 CMIP
 527 esm-hist*. Earth System Grid Federation. Retrieved from <https://doi.org/10.22033/ESGF/CMIP6.7575> doi: 10.22033/ESGF/CMIP6.7575
- 528 Danabasoglu, G., Lamarque, J.-F., Bacmeister, J., Bailey, D. A., DuVivier, A. K.,
 529 Edwards, J., ... Strand, W. G. (2020). The Community Earth System Model
 530 Version 2 (CESM2). *Journal of Advances in Modeling Earth Systems*, 12(2),
 531 e2019MS001916. Retrieved from <https://doi.org/10.1029/2019MS001916>
 532 doi: <https://doi.org/10.1029/2019MS001916>
- 533 Dekker, M. M., von der Heydt, A. S., & Dijkstra, H. A. (2018). Cascading transi-
 534 tions in the climate system. *Earth System Dynamics*, 9(4), 1243–1260. Re-
 535 tried from <https://esd.copernicus.org/articles/9/1243/2018/> doi: 10
 536 .5194/esd-9-1243-2018
- 537 Ditlevsen, P., & Ditlevsen, S. (2023). Warning of a forthcoming collapse of the
 538 Atlantic meridional overturning circulation. *Nature Communications*, 14(1),
 539 4254.
- 540 Eyring, V., Bony, S., Meehl, G. A., Senior, C. A., Stevens, B., Stouffer, R. J., &
 541 Taylor, K. E. (2016, may). Overview of the Coupled Model Intercompari-
 542 son Project Phase 6 (CMIP6) experimental design and organization. *Geosci.
 543 Model Dev.*, 9(5), 1937–1958. Retrieved from <https://gmd.copernicus.org/>
- 544

- articles/9/1937/2016/https://gmd.copernicus.org/articles/9/1937/2016/gmd-9-1937-2016.pdf doi: 10.5194/gmd-9-1937-2016
- Gottschalk, J., Battaglia, G., Fischer, H., Frölicher, T. L., Jaccard, S. L., Jeltsch-Thömmes, A., ... Stocker, T. F. (2019). Mechanisms of millennial-scale atmospheric CO₂ change in numerical model simulations. *Quaternary Science Reviews*, 220, 30–74. Retrieved from <http://www.sciencedirect.com/science/article/pii/S0277379118310473> doi: <https://doi.org/10.1016/j.quascirev.2019.05.013>
- Henson, S. A., Laufkötter, C., Leung, S., Giering, S. L. C., Palevsky, H. I., & Ca- van, E. L. (2022). Uncertain response of ocean biological carbon export in a changing world. *Nature Geoscience*, 15(4), 248–254. Retrieved from <https://doi.org/10.1038/s41561-022-00927-0> doi: 10.1038/s41561-022-00927-0
- Jackson, L. C., Kahana, R., Graham, T., Ringer, M. A., Woollings, T., Mecking, J. V., & Wood, R. A. (2015). Global and European climate impacts of a slow-down of the AMOC in a high resolution GCM. *Climate Dynamics*, 45(11), 3299–3316. Retrieved from <https://doi.org/10.1007/s00382-015-2540-2> doi: 10.1007/s00382-015-2540-2
- Katavouta, A., & Williams, R. G. (2021). Ocean carbon cycle feedbacks in CMIP6 models: contributions from different basins. *Biogeosciences*, 18(10), 3189–3218. Retrieved from <https://bg.copernicus.org/articles/18/3189/2021/> doi: 10.5194/bg-18-3189-2021
- Köhler, P., Joos, F., Gerber, S., & Knutti, R. (2005). Simulated changes in vegetation distribution, land carbon storage, and atmospheric CO₂ in response to a collapse of the North Atlantic thermohaline circulation. *Climate Dynamics*, 25(7), 689. Retrieved from <https://doi.org/10.1007/s00382-005-0058-8> doi: 10.1007/s00382-005-0058-8
- Kwiatkowski, L., Torres, O., Bopp, L., Aumont, O., Chamberlain, M., Christian, J. R., ... Ziehn, T. (2020). Twenty-first century ocean warming, acidification, deoxygenation, and upper-ocean nutrient and primary production decline from CMIP6 model projections. *Biogeosciences*, 17(13), 3439–3470. Retrieved from <https://bg.copernicus.org/articles/17/3439/2020/> doi: 10.5194/bg-17-3439-2020
- Lawrence, D. M., Fisher, R. A., Koven, C. D., Oleson, K. W., Swenson, S. C., Bonan, G., ... Zeng, X. (2019, dec). The Community Land Model Version 5: Description of New Features, Benchmarking, and Impact of Forcing Uncertainty. *Journal of Advances in Modeling Earth Systems*, 11(12), 4245–4287. Retrieved from <https://doi.org/10.1029/2018MS001583> doi: <https://doi.org/10.1029/2018MS001583>
- Lenton, T. M., Held, H., Kriegler, E., Hall, J. W., Lucht, W., Rahmstorf, S., & Schellnhuber, H. J. (2008). Tipping elements in the Earth's climate system. *Proceedings of the National Academy of Sciences*, 105(6), 1786–1793. Retrieved from <https://www.pnas.org/doi/abs/10.1073/pnas.0705414105> doi: 10.1073/pnas.0705414105
- Liu, Y., Moore, J. K., Primeau, F., & Wang, W. L. (2023). Reduced CO₂ uptake and growing nutrient sequestration from slowing overturning circulation. *Nature Climate Change*, 13(1), 83–90. Retrieved from <https://doi.org/10.1038/s41558-022-01555-7> doi: 10.1038/s41558-022-01555-7
- Long, M. C., Moore, J. K., Lindsay, K., Levy, M., Doney, S. C., Luo, J. Y., ... Sylvester, Z. T. (2021). Simulations With the Marine Biogeochemistry Library (MARBL). *Journal of Advances in Modeling Earth Systems*, 13(12), e2021MS002647. Retrieved from <https://doi.org/10.1029/2021MS002647> doi: <https://doi.org/10.1029/2021MS002647>
- Lynch-Stieglitz, J. (2017). The Atlantic Meridional Overturning Circulation and Abrupt Climate Change. *Annual Review of Marine Science*, 9(1), 83–104. Retrieved from <https://doi.org/10.1146/annurev-marine-010816-060415>

- doi: 10.1146/annurev-marine-010816-060415
- Marchal, O., Stocker, T. F., & Joos, F. (1998, jun). Impact of oceanic reorganizations on the ocean carbon cycle and atmospheric carbon dioxide content. *Paleoceanography*, 13(3), 225–244. Retrieved from <https://doi.org/10.1029/98PA00726> doi: <https://doi.org/10.1029/98PA00726>
- McKay, D. I. A., Staal, A., Abrams, J. F., Winkelmann, R., Sakschewski, B., Loriani, S., ... Lenton, T. M. (2022). Exceeding 1.5°C global warming could trigger multiple climate tipping points. *Science*, 377(6611), eabn7950. Retrieved from <https://www.science.org/doi/abs/10.1126/science.abn7950> doi: 10.1126/science.abn7950
- Nielsen, S. B., Jochum, M., Pedro, J. B., Eden, C., & Nuterman, R. (2019, apr). Two-Timescale Carbon Cycle Response to an AMOC Collapse. *Paleoceanography and Paleoclimatology*, 34(4), 511–523. Retrieved from <https://doi.org/10.1029/2018PA003481> doi: <https://doi.org/10.1029/2018PA003481>
- Nohara, D., Yoshida, Y., Misumi, K., & Ohba, M. (2013, mar). Dependency of climate change and carbon cycle on CO₂ emission pathways. *Environmental Research Letters*, 8(1), 14047. Retrieved from <https://dx.doi.org/10.1088/1748-9326/8/1/014047> doi: 10.1088/1748-9326/8/1/014047
- Obata, A. (2007, dec). Climate Carbon Cycle Model Response to Freshwater Discharge into the North Atlantic. *Journal of Climate - J CLIMATE*, 20, 5962–5976. doi: 10.1175/2007JCLI1808.1
- O'Neill, B. C., Carter, T. R., Ebi, K., Harrison, P. A., Kemp-Benedict, E., Kok, K., ... Pichs-Madruga, R. (2020). Achievements and needs for the climate change scenario framework. *Nature Climate Change*, 10(12), 1074–1084. Retrieved from <https://doi.org/10.1038/s41558-020-00952-0> doi: 10.1038/s41558-020-00952-0
- Orihuela-Pinto, B., England, M. H., & Taschetto, A. S. (2022). Interbasin and interhemispheric impacts of a collapsed Atlantic Overturning Circulation. *Nature Climate Change*, 12(6), 558–565. Retrieved from <https://doi.org/10.1038/s41558-022-01380-y> doi: 10.1038/s41558-022-01380-y
- Rahmstorf, S. (2002). Ocean circulation and climate during the past 120,000 years. *Nature*, 419(6903), 207–214. Retrieved from <https://doi.org/10.1038/nature01090> doi: 10.1038/nature01090
- Sarmiento, J. L., Hughes, T. M. C., Stouffer, R. J., & Manabe, S. (1998). Simulated response of the ocean carbon cycle to anthropogenic climate warming. *Nature*, 393(6682), 245–249. Retrieved from <https://doi.org/10.1038/30455> doi: 10.1038/30455
- Schmittner, A. (2005). Decline of the marine ecosystem caused by a reduction in the Atlantic overturning circulation. *Nature*, 434(7033), 628–633. Retrieved from <https://doi.org/10.1038/nature03476> doi: 10.1038/nature03476
- Schmittner, A., & Galbraith, E. D. (2008). Glacial greenhouse-gas fluctuations controlled by ocean circulation changes. *Nature*, 456(7220), 373–376. Retrieved from <https://doi.org/10.1038/nature07531> doi: 10.1038/nature07531
- Smith, R., Jones, P. W., Briegleb, P. A., Bryan, O., Danabasoglu, G., Dennis, M. L., ... Yeager, S. G. (2010). The Parallel Ocean Program (POP) reference manual: Ocean component of the Community Climate System Model (CCSM)..
- Swingedouw, D., Bopp, L., Matras, A., & Braconnot, P. (2007, dec). Effect of land-ice melting and associated changes in the AMOC result in little overall impact on oceanic CO₂ uptake. *Geophysical Research Letters*, 34(23). Retrieved from <https://doi.org/10.1029/2007GL031990> doi: <https://doi.org/10.1029/2007GL031990>
- Tagliabue, A., Kwiatkowski, L., Bopp, L., Butenschön, M., Cheung, W., Lengaigne, M., & Vialard, J. (2021). Persistent Uncertainties in Ocean Net Primary Production Climate Change Projections at Regional Scales Raise Chal-

- 659 lenges for Assessing Impacts on Ecosystem Services. *Frontiers in Climate*,
 660 3. Retrieved from <https://www.frontiersin.org/articles/10.3389/fclim.2021.738224> doi: 10.3389/fclim.2021.738224
- 661 Vellinga, M., & Wood, R. A. (2002). Global Climatic Impacts of a Collapse of the
 662 Atlantic Thermohaline Circulation. *Climatic Change*, 54(3), 251–267. Re-
 663 trieved from <https://doi.org/10.1023/A:1016168827653> doi: 10.1023/A:
 664 1016168827653
- 665 Weijer, W., Cheng, W., Drijfhout, S. S., Fedorov, A. V., Hu, A., Jackson, L. C., ...
 666 Zhang, J. (2019, aug). Stability of the Atlantic Meridional Overturning Cir-
 667 culation: A Review and Synthesis. *Journal of Geophysical Research: Oceans*,
 668 124(8), 5336–5375. Retrieved from <https://doi.org/10.1029/2019JC015083>
 669 doi: <https://doi.org/10.1029/2019JC015083>
- 670 Weijer, W., Cheng, W., Garuba, O. A., Hu, A., & Nadiga, B. T. (2020, jun).
 671 CMIP6 Models Predict Significant 21st Century Decline of the Atlantic
 672 Meridional Overturning Circulation. *Geophysical Research Letters*, 47(12),
 673 e2019GL086075. Retrieved from <https://doi.org/10.1029/2019GL086075>
 674 doi: <https://doi.org/10.1029/2019GL086075>
- 675 Whitt, D. B., & Jansen, M. F. (2020, jul). Slower nutrient stream suppresses
 676 Subarctic Atlantic Ocean biological productivity in global warming. *Pro-
 677 ceedings of the National Academy of Sciences*, 117(27), 15504–15510. Re-
 678 trieved from <https://doi.org/10.1073/pnas.2000851117> doi: 10.1073/
 679 pnas.2000851117
- 680 Wilson, J. D., Andrews, O., Katavouta, A., de Melo Viríssimo, F., Death,
 681 R. M., Adloff, M., ... Ying, R. (2022). The biological carbon pump
 682 in CMIP6 models: 21st century trends and uncertainties. *Proceedings*
 683 *of the National Academy of Sciences*, 119(29), e2204369119. Retrieved
 684 from <https://www.pnas.org/doi/abs/10.1073/pnas.2204369119> doi:
 685 10.1073/pnas.2204369119
- 686 Yamamoto, A., Abe-Ouchi, A., & Yamanaka, Y. (2018). Long-term response of
 687 oceanic carbon uptake to global warming via physical and biological pumps.
 688 *Biogeosciences*, 15(13), 4163–4180. Retrieved from <https://bg.copernicus.org/articles/15/4163/2018/> doi: 10.5194/bg-15-4163-2018
- 689 Zhang, R., & Delworth, T. L. (2005). Simulated Tropical Response to a Substan-
 690 tial Weakening of the Atlantic Thermohaline Circulation. *Journal of Cli-
 691 mate*, 18(12), 1853–1860. Retrieved from <https://journals.ametsoc.org/view/journals/clim/18/12/jcli3460.1.xml> doi: <https://doi.org/10.1175/JCLI3460.1>
- 692 Zhu, J., Zeng, X., Gao, X., & Zhang, H. (2022). Response of Terrestrial Net
 693 Primary Production to Quadrupled CO₂ Forcing: A Comparison between
 694 the CAS-ESM2 and CMIP6 Models. *Biology*, 11(12). Retrieved from
 695 <https://doi.org/10.3390/biology11121693> doi: <https://doi.org/10.3390/biology11121693>
- 696 Zickfeld, K., Eby, M., & Weaver, A. J. (2008, sep). Carbon-cycle feedbacks of
 697 changes in the Atlantic meridional overturning circulation under future at-
 698 mospheric CO₂. *Global Biogeochemical Cycles*, 22(3). Retrieved from
 699 <https://doi.org/10.1029/2007GB003118> doi: <https://doi.org/10.1029/2007GB003118>
- 700
- 701
- 702
- 703
- 704
- 705

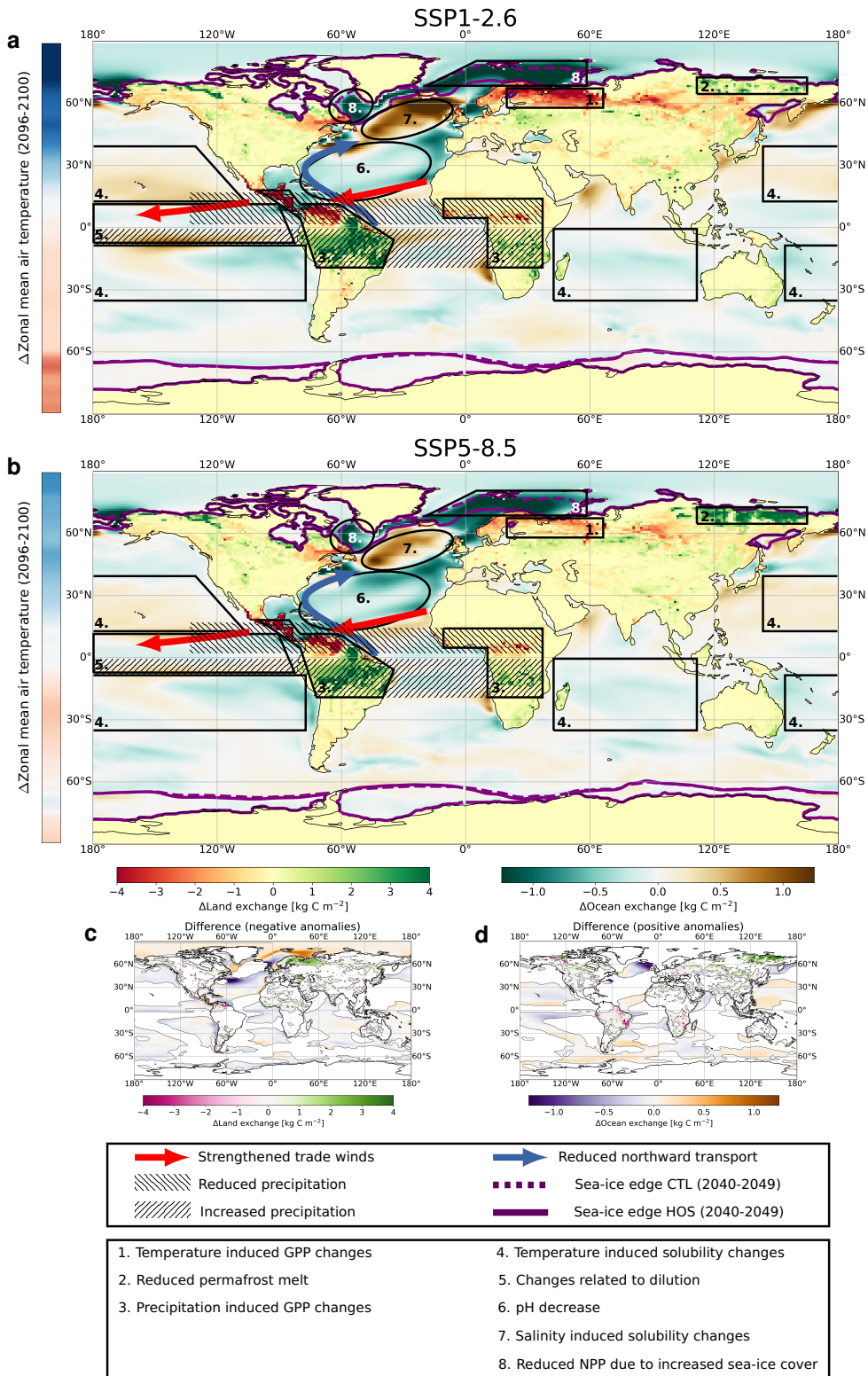


Figure 10. Summarizing figure with dominant mechanisms included for SSP1-2.6 (a) and SSP5-8.5 (b). (a) and (b) represent results from HOS minus the CTL simulations. The sea-ice edge is taken as where the ice fraction is 0.25 and denoted by the purple lines, where dashed lines represent the CTL simulations and solid lines the HOS simulations. The bar at the left shows the difference in zonal mean surface air temperature averaged over 2096-2100 between HOS and CTL. The scaling of this bar is between -2.5°C (dark blue) and 2.5°C (dark red). (c) The difference between SSP5-8.5 (b) and SSP1-2.6 (a) for the regions where (b) is negative. Negative values represent a higher negative anomaly in SSP5-8.5 compared to SSP1-2.6. (d) as in (c) but for positive anomalies. Positive values represent a higher positive anomaly in SSP5-8.5 compared to SSP1-2.6. The color bars in (c) and (d) apply to both subfigures.